

In hot water: effects of temperature-dependent interiors on the radii of water-rich super-Earths

Scott W. Thomas & Nikku Madhusudhan

Institute of Astronomy, University of Cambridge, Madingley Road, Cambridge CB3 0HA, United Kingdom

January 2016

ABSTRACT

Observational advancements are leading to increasingly precise measurements of super-Earth masses and radii. Such measurements are used in internal structure models to constrain interior compositions of super-Earths. It is now critically important to quantify the effect of various model assumptions on the predicted radii. In particular, models often neglect thermal effects, a choice justified by noting that the thermal expansion of a solid Earth-like planet is small. However, the thermal effects for water-rich interiors may be significant. We have systematically explored the extent to which thermal effects can influence the radii of water-rich super-Earths over a wide range of masses, surface temperatures, surface pressures and water mass fractions. We developed temperature-dependent internal structure models of water-rich super-Earths that include a comprehensive temperature-dependent water equation of state. We found that thermal effects induce significant changes in their radii. For example, for super-Earths with 10 per cent water by mass, the radius increases by up to $0.5R_{\oplus}$ when the surface temperature is increased from 300 to 1000 K, assuming a surface pressure of 100 bar and an adiabatic temperature gradient in the water layer. The increase is even larger at lower surface pressures and/or higher surface temperatures, while changing the water fraction makes only a marginal difference. These effects are comparable to current super-Earth radial measurement errors, which can be better than $0.1R_{\oplus}$. It is therefore important to ensure that the thermal behaviour of water is taken into account when interpreting super-Earth radii using internal structure models.

1 INTRODUCTION

One of the most interesting classes of planets today is the class of super-Earths, planets with masses between 1 and $10M_{\oplus}$. With no analogues in the solar system, it is not known whether they are scaled up rocky planets or scaled down Neptunes. About 40 super-Earths with measured masses and radii are currently known. Their radii range from 1 to $7R_{\oplus}$.¹ With the potential to have moderate atmospheres and plate tectonics, super-Earths represent an important class of planets in the broader context of planetary diversity and planetary habitability (Haghighipour 2011; Baraffe et al. 2014).

Recent observational advancements are leading to increasingly precise measurements of masses and radii of these small planets. Such measurements are being used with internal structure models to place constraints on the interior compositions of super-Earths. Many planets are well-described by multi-layer models consisting of iron, silicates, and water (e.g. Valencia et al. 2006; Fortney et al. 2007; Sotin et al. 2007; Seager et al. 2007) and others have included layers of hydrogen or other volatiles to explain the inflated radii

of some super-Earths (e.g. Rogers & Seager 2010a; Lopez et al. 2012). Given the high-precision radii measurements, it is now critically important to quantify the dependence of predicted radii of super-Earth models on the various model assumptions.

Our goal is to quantify the effects of temperature-dependent internal structure models on the predicted radii of super-Earths. An understanding of the effects of temperature on the internal structures of planets is especially relevant as our observational capabilities for measuring radii and masses improve. In particular, we are interested in understanding to what degree the observable radius of a planet may be affected by thermal expansion of its interior. We use water as a case study for this, focusing on super-Earth planets consisting of a rocky Earth-like core underneath a heated water layer.

The remainder of this section provides an overview of how these planetary interior models can be useful, why we expect temperature-dependent models to be different and why water-rich planets make interesting test cases for assessing whether this temperature dependence is significant.

¹ This number is taken from the exoplanets.org database (confirmed planets only).

1.1 Planetary interior models

As atmospheric characterisation techniques improve, the question of what lies beneath the atmosphere has naturally arisen. We care about planetary interiors because they are linked to the formation history of the planet, because they are shaped by and shape the planetary atmosphere and because they are key to answering questions about habitability (Sotin et al. 2010). Understanding these exoplanets also allows us to place our own Earth into context: how unique are we? We therefore seek to understand, if not the interiors of individual exoplanets, at least something about broad classes of planets. But it is here that we are confronted by a lack of data, because we have very little ability to directly probe the interiors of exoplanets.

This lack of a rich source of observational data for planetary interiors means that we rely strongly on models. Even inside our solar system, our knowledge of planetary interiors is limited by the indirect ways in which we can probe them. On Earth we have the advantage of seismic measurements, and in our solar system we have various gravitational moments to constrain interior structures. Outside the solar system we have only the masses and radii of planets to work with. Models from first principles (numerical or analytical models based on the physics of solid and liquid spheres) therefore dominate the field.

Planetary interior models are a worthwhile starting point to make sense of the limited observational data we have. These models are inspired by earlier successes with stellar structure models, which are key to interpreting observations of stars. Others had previously considered the internal structures of planets in our solar system (for example, Hubbard & MacFarlane 1980), but the study often taken as the base for planetary interior modelling is by Zapolsky & Salpeter (1969) who constructed mass–radius relations for large homogeneous isothermal spheres. A number of internal structure models have been developed for exoplanets, starting with early works a decade ago (e.g. Valencia et al. 2006; Fortney et al. 2007; Sotin et al. 2007; Seager et al. 2007). The ever-increasing number of known exoplanets, many of which have both mass and radius measurements, are a diverse and interesting set of objects to which to apply these models.

The first way in which planetary interior models can be useful is to make broad inferences about the structure of a planet. There is some information available about any planet despite an inherent degeneracy between different compositions. We can immediately exclude certain classes of models: for example, small planets with large radii must almost certainly have large hydrogen envelopes. We can also take more sophisticated approaches. Sotin et al. (2007) modelled planets by fixing their compositions based on the properties of the host star. Madhusudhan et al. (2012) argued for a carbon-rich interior in the exoplanet 55 Cnc e based on its carbon abundance and on its density matching that of pure carbon. Dorn et al. (2015) also showed that mass and radius alone can constrain the size of a planet’s core if we assume it is pure iron.

We can also hope to make progress in a statistical sense by examining populations of planets. Such progress is possible even if we are unable to pin down the precise structure of an individual planet. There are promising advances in

this direction already. These usually involve inverse Bayesian analyses. For example, Rogers (2015) investigated the size demographics of planetary populations and set an approximate boundary of $1.6 R_{\oplus}$ beyond which planets are likely to have gaseous envelopes.

Finally, interior structure models may be useful when combined with prescriptions for planetary formation. Morasini et al. (2012) took this approach, combining interior structure calculations with models of the protoplanetary disk to produce synthetic populations of planets. Lopez et al. (2012) also made model planets and explored how they evolve and lose mass through time (see also Owen & Wu 2015).

If we are to use mass and radius to constrain the interior structure of a planet, we should ensure that our models are precise and accurate. But more importantly, we should understand where our models need to be precise and accurate and where such effort is wasted. We therefore require a thorough understanding of what factors can affect the mass–radius relation. We also need to know to what extent we are able to invert the relation to determine a composition.

The internal structure of a planet is not well-constrained by its mass and radius alone (Rogers & Seager 2010a). However, we know that we can obtain some compositional constraints from observations of the planet and its host star. Above, we mentioned works by Sotin et al. (2007) and Madhusudhan et al. (2012), who used host star information in this way. Dorn et al. (2015) also used probabilistic models, incorporating the host star chemical abundances, to conclude that “uncertainties on mass, radius, and stellar abundance constraints appear to be equally important.” Grasset et al. (2009) indicated the need for good radius measurements, especially for dry silicate-rich planets for which numerical models can provide radius estimates to precisions of less than 5 per cent. Unterborn et al. (2015) used a mineral physics toolkit to perform a sensitivity analysis for rocky super-Earths, concluding that the mass–radius relationship is most strongly altered by the core radius and the presence of light elements in the core.

The presence of an atmosphere could also contribute significantly to the observed radius. Rogers & Seager (2010b) have modelled isothermal super-Earth interiors overlaid by a volatile atmosphere. Additionally, Valencia et al. (2013) considered coupled atmosphere–interior models, which also included atmospheric mass loss, and explored the dependence of radii on various model parameters such as the irradiation, water content and metallicity. The effect of an atmosphere is important, especially given that observations can probe spectral ranges where atmospheric absorption could be significant (Madhusudhan & Redfield 2015).

Though the factors above are all important, the effect of temperature on the mass–radius relation has not been thoroughly explored (but see e.g. Valencia et al. 2013). This is for several reasons. First, its effects are thought to be relatively minor in the first place: Howe et al. (2014) estimate that the effect of thermal corrections on an iron–silicate planet’s radius is approximately 5 per cent. Grasset et al. (2009) also describe how the radius of an Earth-like planet is not strongly affected by temperature changes. If the effect is small compared with current observational uncertainties, it is not necessarily relevant. Secondly, modelling is easier if we assume zero-temperature or isothermal spheres of mate-

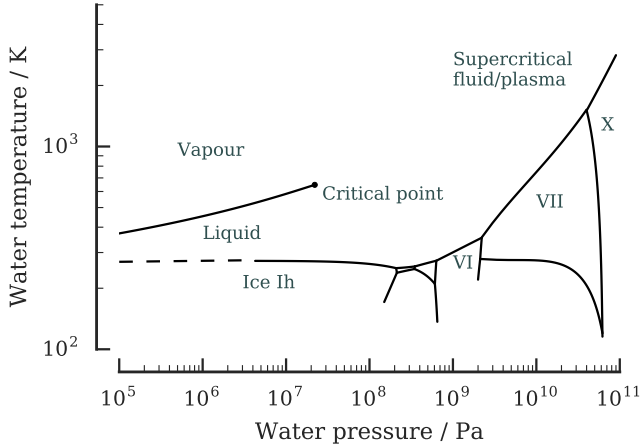


Figure 1. Phase diagram of water. Water has a rich and interesting phase structure. Here we show some of the key phases which are relevant when modelling a watery planet: liquid, vapour, and solid ice Ih, but also more exotic phases such as the high-pressure ices. Lines mark the boundaries of each phase as given by Choukroun & Grasset (2007) and Wagner & Pruß (2002).

rial, because we do not have to deal with energy transport within the planet. Finally, the data on thermal expansion of heavy elements are sparse at the high temperatures and pressures characteristic of planetary interiors (Baraffe et al. 2008). Therefore mass–radius relations or models of individual planets traditionally had no temperature dependence at all (Zapolsky & Salpeter 1969; Seager et al. 2007) but it is increasingly being included and thermal effects on radii are being explored (for example, see Valencia et al. 2013).

1.2 Temperature dependence of water-rich planets

The degree to which thermal structure may affect the properties of a water-rich planet has not yet been well studied. Super-Earth planets with significant water layers, sometimes called waterworlds, provide an interesting testbed for our investigation. They may display more significant variation in their properties, both observable and internal, than purely Earth-like (iron and silicate) planets. They are therefore a worthwhile target for this study.

Water presents an opportunity to assess thermal effects in a material that has a rich and interesting phase structure across a large temperature and pressure range (Fig. 1). At low temperature and pressure, water exists as a liquid, vapour, or solid (Ice Ih). At high pressure, it takes on a number of alternate ice forms (Ice V, VI, VII, X, etc.) (Choukroun & Grasset 2007). It can also exist as a low-density supercritical fluid or superheated vapour. This all means that the behaviour of water layers is thermally interesting. The behaviour of water is also strongly linked to questions of habitability because Earth-sized solid planets with oceans provide the best approximation to the one planet known to harbour life.

Others have previously investigated the structures of planets containing a significant water component. For example, Ehrenreich et al. (2006) studied the internal structure of the exoplanet OGLE 2005-BLG-390Lb, modelling

the phase changes throughout. Zeng & Sasselov (2014) chose to explore evolutionary effects, following the phase transitions within model water-rich planets. They comment that “[phase] transformations may have a significant effect on the interior convective pattern and also the magnetic field of such a planet, but they may only affect the overall radius slightly.” Our present study addresses the question of exactly how much temperature variations affect the structure and radius of water-rich planets and whether such effects are observable.

2 METHOD

Guided by the motivations above, we quantified the thermal effects in super-Earths which contain significant amounts of water. By *thermal effects* we mean three effects in particular. First, we mean the thermal expansion of a heated water layer on the surface or within the planet’s interior: this contrasts with models which treat the planets as cold spheres. Secondly, we mean any temperature gradient established within the planet: this is in contrast to the isothermal case. And thirdly, we expect phase transitions within the water layer if the temperature and pressure cross one of the boundaries between different phases of water seen in Fig. 1.

To quantify these effects required several steps. First, we selected an appropriate temperature-dependent equation of state. We built planetary interior structure models that included this equation of state. We incorporated a realistic temperature gradient into these models. Finally, we explored the model parameter space. In particular, we compared the mass–radius relationships for these water worlds across a range of surface pressures, surface temperatures and interior compositions.

In this section, we first explain how we built models of super-Earth interiors: we constructed layered one-dimensional models of water, rock and iron in varying proportions. We discuss our approach to the temperature structure: we treated the temperature gradient as adiabatic and self-consistently calculated it from the equation of state, an approach which naturally handles phase boundaries within the water layer. We explain how we used these models to construct temperature-dependent mass–radius relations for both homogeneous and layered planets. Next we present the equation of state for water that we used. It is comprehensive over the pressure and temperature range relevant to super-Earth interiors. We highlight the difficulty of dealing with disparate sources of experimental and theoretical data in different phases, as well as sources of uncertainty within the equation of state. Finally, we present comparisons with previous works to verify that our structural modelling code works appropriately.

2.1 Interior structure modelling

We constructed temperature-dependent planetary interior models of water-rich super-Earths. We considered the planet to be spherically symmetric, non-rotating and non-magnetic. The following equations govern the structure of such a planetary interior.

2.1.1 Planetary structure equations

The mass continuity equation,

$$\frac{dr}{dm} = \frac{1}{4\pi r^2 \rho}, \quad (1)$$

links r , the radius of a spherical shell, to the mass m interior to the shell and the density ρ of the shell. The equation of hydrostatic equilibrium,

$$\frac{dP}{dm} = -\frac{Gm}{4\pi r^4}, \quad (2)$$

where P is the pressure at the shell and G is the gravitational constant, ensures a balance of pressure and gravity. The equation of state,

$$\rho = \rho(P, T), \quad (3)$$

is used to calculate the density of the material in question from its pressure and temperature T .

Previous models of super-Earth interiors have treated temperature gradients within the planet in a number of ways. From simple to complex, these include:

1. Isothermal models, which use only the equations above and an isothermal equation of state of the form $\rho = \rho(P)$. This is the approach taken by [Seager et al. \(2007\)](#).

2. Simple temperature prescriptions:

- a) One may assume a fixed temperature–pressure relation $T = T(P)$ so as to reduce the equation of state to the form $\rho = \rho(P)$ and then use the equations above. For example, [Zeng & Sasselov \(2013\)](#) chose the melting curve of water for this purpose.

- b) Or one may choose a temperature profile $T = T(r)$ for the planet (perhaps scaled appropriately to an internal or external boundary temperature) and then use the equations above.

3. An adiabatic or conductive temperature gradient or some combination of the two. For example, [Valencia et al. \(2010\)](#) used a convective interior with conductive boundary layers.

4. A full treatment, which adds an energy transport equation to the equations above then self-consistently solves this with a prescription for luminosity. For example, [Wagner et al. \(2011\)](#) modelled an adiabatic core underneath a radiogenically heated mantle.

We did not explicitly handle energy transport in the manner of the fourth option. Instead we chose the third approach and assumed an adiabatic (isentropic) temperature gradient throughout the planet. The equation for the adiabatic temperature gradient, as given by [Milone & Wilson \(2014\)](#), is

$$\frac{dT}{dr} = -\frac{T\alpha g}{c_p}. \quad (4)$$

where $g = Gm/r^2$ is the gravity at the shell, c_p is the isobaric heat capacity and α is the volumetric thermal expansion coefficient. This is sometimes written α_V and is defined as the fractional increase in volume per unit temperature increase,

$$\alpha = \frac{1}{V} \left. \frac{\partial V}{\partial T} \right|_p = - \left. \frac{\partial \ln \rho}{\partial \ln T} \right|_p. \quad (5)$$

Our sources for these latter two coefficients are detailed in

our equation of state section. Equation 4 combined with equation 1 gives the temperature gradient in terms of the mass co-ordinate,

$$\frac{dT}{dm} = -\frac{T\alpha Gm}{\rho c_p 4\pi r^4}. \quad (6)$$

2.1.2 Solving the structural equations

Together, equations 1, 2, 3 and 6 define a structural model: three ordinary differential equations and an equation of state linking pressure, temperature and density. The choice of how to solve this system depends on one's aim. A common approach has been to treat it as a boundary value problem; that is, to integrate the structural equations from initial conditions at the surface or centre of the planet. For example, [Seager et al. \(2007\)](#) approached the isothermal problem (equations 1, 2 and 3 only) from the inside out, choosing appropriate central pressures at the ($r=0, m=0$) boundary and building their models outward from there. We instead integrate from the outside in, an approach taken by several others (e.g. [Rogers & Seager 2010a](#); [Madhusudhan et al. 2012](#)). This has the advantage of allowing us to specify the surface temperature and pressure as boundary conditions. These surface boundary conditions are more closely linked to observable parameters than the central pressure and temperature.

We used a Lagrangian system, where the mass interior to a given shell is the independent variable; this is reflected in equations 1, 2 and 3. It is in contrast to the Eulerian co-ordinate system used by [Seager et al. \(2007\)](#), who take the radius r as the independent variable. [Rogers & Seager \(2012\)](#) claim that this formulation is more stable under numerical integration. We also found it more convenient to be able to specify differentiated planets in terms of mass fractions rather than radial distances.

We solved this boundary value problem using a shooting method². This method used a series of trial solutions, adjusting the initial conditions as necessary based on the difference between the expected and actual values at the end of the integration domain. For the initial trial solution, we specified the surface boundary conditions: total planetary mass M , surface pressure $P(M)$, and surface temperature $T(M)$. We also specified a search bracket for the radius $[R_1(M), R_2(M)]$. Our code³ used a fixed-step fourth-order Runge–Kutta integrator to solve the system of differential equations above. In each successive trial, it iteratively adjusted the radius boundary condition $R(M)$ according to the bisection root-finding method to ensure that the radius approached zero as the mass approached zero. We further required that r remained positive: this avoided any numerical difficulty arising from the behaviour of the equations at $r=0$. We deemed the system to be converged acceptably when the central radius $r(m=0)$ was between 0 and 100 m.

² For an example implementation, see [Press \(2007\)](#), chapter 18.

³ Our code was written in [Julia](#).

2.1.3 Mass–radius relations with thermal expansion and multiple layers

We used our models to produce mass–radius relations for homogeneous spheres of water as well as differentiated multi-layer models. We did this first for the homogeneous isothermal case (in the vein of [Zapolsky & Salpeter 1969](#)) and then extended our models to include an adiabatic temperature gradient. Our differentiated multi-layer models included a water layer on top of a silicate mantle and an iron core. To do this, they treated the equation of state, equation 3, as piecewise in the mass co-ordinate. For example, consider a model which has a 5 per cent (by mass) water layer on top of a silicate mantle. For this model, we begin by evaluating equation 3 using the water equation of state. We then switch to the silicate equation of state once m , the mass interior to the spherical shell in equations 1, 2 and 6, drops below 95 per cent of the planetary mass. It is possible to choose the integration grid such that this occurs exactly at the end of an integration step. However, in practice a sufficiently fine grid is also acceptable.

We ignored thermal effects within the iron and silicate layers. The effect of thermal expansion in these solids is thought to be low (see [Seager et al. 2007](#); [Grasset et al. 2009](#)). Including the expansion effects of these materials would be very simple, but we have not yet collated the equation of state data which would enable us to do so. Because we ignored thermal expansion in these layers, we modelled them as isothermal, which follows from setting $\alpha = 0$ in equation 6 so that $dT/dm = 0$.

We aimed to accurately capture the density change of water at its phase boundaries. Our equation of state for water therefore included its phase transitions, which appear as density discontinuities in pressure–temperature space. When calculating the adiabatic temperature profile, we enforced temperature and pressure continuity at these phase boundaries. We did this by ensuring that the equation for the adiabatic temperature gradient, equation 6, was finite and continuous. This effectively split the adiabatic temperature profile into several different sections, consisting of one separate adiabat for each phase and meeting at the phase boundaries of water. By handling each phase separately, we avoided the numerical difficulty of taking a derivative (equation 5) across a density discontinuity.

We note that it is possible to fix the radius and let another parameter vary instead. This could be the mass, surface temperature, surface pressure or the position of a layer boundary within the planet. Other studies have used this approach to infer potential compositions for planets of known mass and radius. We instead left the radius free to investigate how much it was affected by the water layer’s thermal expansion. This was the primary goal of this study.

2.2 Equation of state

As the goal of this study was to investigate thermal effects, we required a temperature-dependent equation of state for water. This allowed us to treat thermal expansion self-consistently in our models. We synthesized an equation of state for water from the best available experimental and theoretical data over a wide range of pressure and temperature.

2.2.1 Previous equations of state for water

There was no single comprehensive equation of state data set available for water over the entire pressure and temperature range relevant to super-Earth interiors. Previous studies have approached this problem by stitching together equations of state which are valid for different pressure regimes. For example, [Seager et al. \(2007\)](#) took this approach with water, combining three temperature-independent equations of state for ice VII:

- the Birch–Murnaghan equation of state at low pressures,
- density functional theory calculations at intermediate pressures and
- the Thomas–Fermi–Dirac model at very high pressures.

The piecewise function defined in this way is appropriate across a wide pressure range.

This pressure piecewise approach neglects temperature dependence in the equation of state but provides a robust approximation that is easy to evaluate. In some cases, stitching the data in this fashion has revealed that a simpler functional form works just as well. For example, this is the case in the “polytropic equation of state” used by [Seager et al. \(2007\)](#). Such simple functional forms for the equation of state have been used successfully to model planets as cold spheres since the work of [Zapolsky & Salpeter \(1969\)](#). In other cases, a more detailed functional form is needed to capture the behaviour of the material fully; this is especially true if it undergoes phase transitions. For example, the IAPWS formulation described by [Wagner & Pruß \(2002\)](#) uses a complicated series of equations fitted to various sources of experimental data for the behaviour of water in the vapour and liquid phases.

In choosing equations of state, previous authors have taken similar approaches to the stitching technique above. Although the choice of the exact equations has varied as new experimental data were released, few of these studies included thermal expansion. [Howe et al. \(2014\)](#) provided a comprehensive overview of the equations of state chosen in previous works to model planetary interiors. They included several different materials of interest for planetary interiors: water ice, iron, and silicates. We repeated this exercise, focusing exclusively on the water equations of state across all its phases. Table 1 summarises our findings.⁴

2.2.2 Our equation of state

We extended the piecewise approach described above to include temperature as a second dimension in parameter space. We drew from a number of the sources of data listed in Table 1. Our stitched equation of state is valid over a wide domain: its temperature domain is from 275 K to 24000 K, and its pressure domain is from 10^5 Pa (1 bar) upwards. Our approach was similar to that of [Senft & Stewart \(2008\)](#), who generated a “5-Phase” equation of state across different liquid, vapour, and ice phases. However, their work focused on the lower temperatures needed to model impact craters. We

⁴ Where abbreviations are used in this table and Table 2, Table 3 indicates from which studies they come.

Table 1. Previous studies on planetary interior structures use a variety of equations of state for water.

Work(s)	Water equation of state used
Baraffe et al. (2008); Baraffe et al. (2014)	TFD, BME, MGD
Fortney et al. (2007)	Simple power law from Hubbard & MacFarlane (1980)
Fortney & Nettelmann (2009)	H ₂ O-REOS
Grasset et al. (2009)	MGD; Vinet; BME; TFD; ANEOS; Belonoshko & Saxena (1991)
Guillot (1999)	Hubbard & Marley (1989)
Howe et al. (2014)	Vinet
Hubbard & MacFarlane (1980)	Simple power law
Hubbard & Marley (1989)	Exponential polynomial EOS without temperature dependence
Lopez et al. (2012)	H ₂ O-REOS
Madhusudhan (2012)	BME
More et al. (1988)	Quotidian EOS (ion EOS with Thomas–Fermi model)
Nettelmann et al. (2008)	LM-REOS
Nettelmann et al. (2011)	H ₂ O-REOS
Redmer et al. (2011)	French et al. (2009)
Rogers & Seager (2010b)	IAPWS; IAPWS extrapolations; TFD
Seager et al. (2007); Rogers & Seager (2010a); Zeng & Sasselov (2014)	Low-temperature polytropic EOS
Senft & Stewart (2008)	IAPWS; Feistel & Wagner (2006); Stewart & Ahrens (2005); BME
Sotin et al. (2007); Sotin et al. (2010)	BME with thermal expansion (MGD)
Valencia et al. (2006)	BME with thermal expansion
Valencia et al. (2010)	French et al. (2009); SESAME
Vazan et al. (2013)	Quotidian EOS; TFD
Wilson & Militzer (2012); Wilson et al. (2013)	DFT
Zeng & Sasselov (2013)	Frank et al. (2004); French et al. (2009); TFD

have explicitly included much higher temperatures so as to capture the behaviour of large super-Earth planets: we expect the cores of these to reach thousands of Kelvin. Valencia et al. (2010) also constructed a similar equation of state, though using only data from SESAME and the IAPWS formulation.

We endeavoured to choose equations of state that were most representative of the thermal behaviour of water across this temperature and pressure domain. We were guided by two principles in doing so. First, as demonstrated in Fig. 3, we expect thermal expansion effects to approach zero as the pressure increases: this is a consequence of the equations of state approaching the high-pressure TFD limit. There are significant temperature effects at lower pressures, and it is these effects we expected to be most important in our

Table 2. We used a variety of equations of state in our final models. “Tabular” indicates that we interpolated between values specified in the paper. “Functional” indicates that we used the functional form given in the paper.

Equation of state	Type	Region of validity
IAPWS	Tabular	Vapour and liquid phases; 0.05 to 1000 MPa and 252.462 to 1273 K
French et al. (2009)	Tabular	Superionic, plasma and high-pressure ice phases; 79 to 9.87×10^6 MPa and 1000 to 24000 K. We did not use table VIII from this work, as this low-density data disagrees with the IAPWS formulation.
Feistel & Wagner (2006)	Tabular	Ice Ih; 0 to 200 MPa and 0 to 273 K
Sugimura et al. (2010)	Tabular	Ice VII; 18880 to 50250 MPa and 431 to 881 K
Vinet + MGD correction using parameters from Fei et al. (1993)	Functional	Ice VII
TFD	Functional	Ice X
Seager et al. (2007)	Functional	Ice VIII–X transition
Choukroun & Grasset (2007)	Functional	Ices I, III, V, VI; phase boundaries as specified by Dunaeva et al. (2010)
IAPWS extrapolations	Functional	Remaining regions

study. Secondly, we aimed for a full treatment of density changes over phase boundaries. Accordingly, we used the phase boundaries specified by Dunaeva et al. (2010) to divide the temperature–pressure phase space into regions corresponding to different phases of water. We then chose an appropriate equation of state to represent each phase.

Our equation of state is for pure water only. Others have investigated how impurities may affect the equation of state and the planet’s properties. For example, Levi et al. (2014) included a methane component in their models, resulting in a new phase of water (filled ice) which changes the planet’s thermal profile. They note that, while neglecting volatiles is an impediment to understanding the planet’s atmosphere, pure water models may be sufficient for planetary mass–radius relations.

In selecting the equations of state we were often faced with choices between different sources of data. The exact behaviour of water at very high pressures is still uncertain and experimental and theoretical results are sometimes in conflict (Baraffe et al. 2014). Ensuring absolute accuracy of the chosen equations of state was therefore a secondary priority. In general, we preferred more recent data to older data, we prioritised measured and tabulated values over functional approximations, and we chose representations that included temperature dependence over those that did not. In the following paragraphs, we describe our equation of state choices and summarise them in Table 2.

Liquid and vapour: The behaviour of water in the liquid and vapour phases is well understood and there are plenty

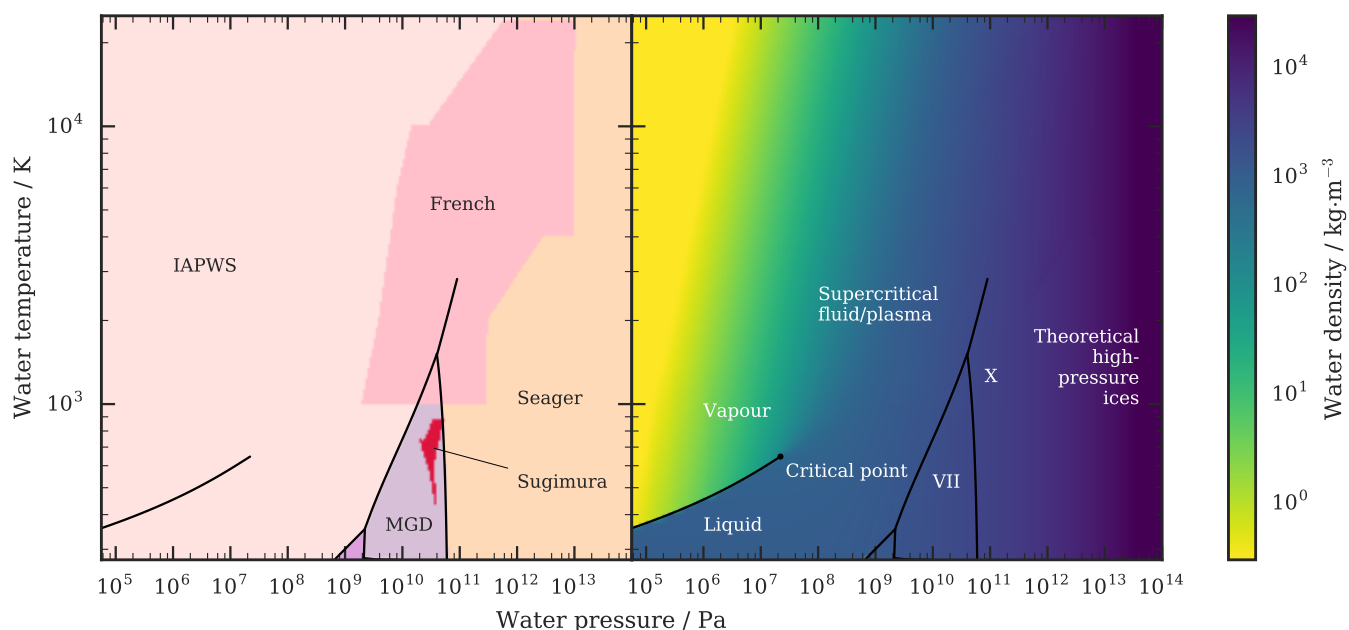


Figure 2. Phases and data sources for our water equation of state. Our equation of state covers a wide range of temperature–pressure space. On the left, we show some of the our key data sources we used, and their regions of validity: the IAPWS formulation by [Wagner & Pruß \(2002\)](#); the theoretical calculations of [French et al. \(2009\)](#); the piecewise equation of state described by [Seager et al. \(2007\)](#); the Mie–Grüneisen–Debye (MGD) thermal correction approach for ice VII in [Sotin et al. \(2007\)](#); and the measurements of [Sugimura et al. \(2010\)](#), which cover a small region of ice VII. We also show the relevant phase boundaries. On the right, we show the density variation across the entire pressure–temperature range. The density of water is more strongly affected by pressure across the range we consider, but temperature also affects its density too, especially across the liquid–vapour phase boundary and in the supercritical region.

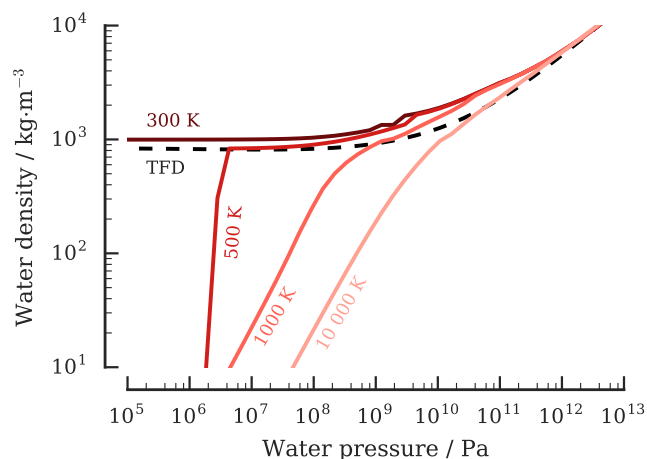


Figure 3. Comparison of our equation of state with the high-pressure limit. The TFD (Thomas–Fermi–Dirac) equation of state is increasingly accurate in the high-pressure limit, where temperature effects on the water density disappear. We also show temperature contours of our water equation of state. The TFD, which has no temperature correction, is a poor approximation of the behaviour of water at low pressures, especially across the liquid–vapour phase boundary (vertical lines). But all other choices of equation of state approach the TFD at high pressures, and so it is appropriate in the TPa region and beyond.

of data available. We were unable to gain access to the SESAME tables of [Lyon & Johnson \(1992\)](#) because there are restrictions on the distribution of this data to non-US

nationals. Instead, to represent water liquid and vapour, we selected the IAPWS (International Association for the Properties of Water and Steam) formulation ([Wagner & Pruß 2002](#)), which provides both tabular and functional data for water in these phases. These are well-tested and validated by years of experiments. [Wagner & Pruß \(2002\)](#) also claim that the functional forms can be extrapolated outside the range of the tables. We implemented the functional relationships between temperature, density and pressure. Where appropriate, we numerically inverted these to give a relation of the form $\rho = \rho(P, T)$. We then tested these against the tables to verify that we had replicated them correctly.

Ice VII: We explicitly chose a temperature-dependent formulation because we expected ice VII to form a significant fraction of the planet in the cases where the water layer is large. This temperature-dependent formulation is in contrast to other studies which have assumed that the ice VII layer is isothermal: for example, [Rogers & Seager \(2010b\)](#) assumed no expansion in all solid layers, choosing to include temperature effects only in the gaseous and liquid phases.

The best temperature-dependent formulation we found for ice VII was the Mie–Grüneisen–Debye (MGD) thermal correction approach described by [Sotin et al. \(2007\)](#). We used a Vinet equation of state with this thermal correction, taking the coefficients of [Fei et al. \(1993\)](#), within the ice VII region delimited by the phase boundaries of [Dunaeva et al. \(2010\)](#). However, we preferred the more recent tabulated measurements of [Sugimura et al. \(2010\)](#) wherever these were applicable; these are shown within the ice VII region in Fig. 2.

Supercritical fluid and plasma: French et al. (2009) presented quantum molecular dynamics simulations of high-temperature and high-pressure plasma, ice, and superionic fluid phases of water. We used their tables in the region beyond 1000 K and 1.86×10^9 Pa. Lopez et al. (2012) noted that this region has recently been probed by laboratory experiments thanks to Knudson et al. (2012), who strongly advocate “that [the French equation of state] be the standard in modeling water in Neptune, Uranus, and ‘hot Neptune’ exoplanets.”. These temperatures and pressures are also relevant to the interiors of super-Earths. We did not use the low-density tables that they presented separately because these differ significantly from the IAPWS results in the same temperature and pressure range.

Low-temperature ices: For completeness, our equation of state includes low-pressure ice Ih from Feistel & Wagner (2006) as well as higher-pressure ices such as ice III, V and VI. We took the phase boundaries from Dunaeva et al. (2010) and used the temperature-dependent formulations for these ices by Choukroun & Grasset (2007).

Ice X and beyond: We adopted the piecewise equation of state of Seager et al. (2007) to describe the transition from ice VII to ice X and beyond. This does not include any temperature dependence: any interesting phase behaviour of ice at these high pressures is increasingly theoretical and unconfirmed by experiment. Temperature effects approach zero at these high pressures anyway (Fig. 3), so we used the Thomas–Fermi–Dirac equation of state for all regions beyond 7686 GPa which were not covered by one of the other regions listed above.

Other regions: Finally, we filled in all other regions according to the IAPWS formulation or extrapolations thereof. In practice, the only regions not covered above were low-pressure and high-temperature vapour regions, which we do not expect to be relevant for our super-Earth interior models.

2.2.3 Dealing with fragmented data

We made no attempt to smooth or otherwise interpolate between the different sources of data described above. This approach means that sharp density changes across phase boundaries are well-represented in the final equation of state. This is desirable so that we may examine the differentiation that results solely from phase transitions. It also results in some artificial density discontinuities at the boundaries between different data sets. We believe that this has not affected the results: these discontinuities are minor compared with the density variations within each phase of water and, in most cases, we also bounded the domain of each data set to that of a particular phase.

Because we used disparate sources of data, we evaluated the density at a given temperature and pressure in different ways depending on the data source. Although we did not smooth or interpolate *between* data sets, we needed to interpolate some data sources *within* the data set. Where data were published in tabulated form on a structured grid, we

Table 3. Sources for the abbreviated equation of state designations used in this paper.

Equation of state	Source
ANEOS	Thompson & Lauson (1972)
BME	Birch–Murnaghan equation of state; see Poirier (2000)
DFT	Density functional theory; refers to theoretical calculations which multiple authors have performed
H ₂ O-REOS	Nettelmann et al. (2011); includes IAPWS, SESAME, French et al. (2009), Feistel & Wagner (2006)
IAPWS	Wagner & Pruß (2002)
LM-REOS	Nettelmann et al. (2008) (precursor to H ₂ O-REOS)
MGD	Mie–Grüneisen–Debye thermal pressure expansion; described in Sotin et al. (2007)
SESAME	Lyon & Johnson (1992)
TFD	Thomas–Fermi–Dirac; described in Salpeter & Zapolsky (1967)
Vinet	Vinet et al. (1987)

used simple two-dimensional linear interpolation⁵ to evaluate the equation of state at points not lying on the grid. Where data were published as unstructured points, we used barycentric interpolation on the mesh of Delaunay triangles⁶ defined by these points. We also used this Delaunay mesh to determine if a given (P, T) pair lay within the domain of a particular equation of state, allowing us to fall back to another equation of state if necessary. We evaluated functional forms of the equation of state as is, defining their domain by means of a bounding box or a polygon in (P, T) space taken from the phase boundaries of Dunaeva et al. (2010).

Some of the equations of state used in this final synthesized version were much simpler than others. This meant that the evaluation time varied from point to point, from very quick table lookups and interpolation to the slower IAPWS formulae. In addition, any equation of state that was specified in the inverse form $P = P(\rho, T)$ needed to be numerically inverted to give the canonical form $\rho = \rho(P, T)$ used in our models. To avoid duplicating this calculation unnecessarily, we re-sampled the final equation of state on to a 256 by 256 pressure–temperature grid. Pre-computing and tabulating the data in this way saved significant time. In our trials, the resolution of the grid barely altered the properties of the planetary models. This suggests that the density behaviour within a single phase region was more important than any effects across phase boundaries that might be lost by sampling from this discrete grid.

The equation of state we used necessarily has some uncertainty in it, especially in regions near the critical point of water (Wagner & Pruß 2002) and at high temperatures and pressures where there are sometimes conflicting experimental and theoretical data (Baraffe et al. 2008). The error in the equation of state varies depending on the original data source. For the region encompassed by the IAPWS data

⁵ For multidimensional linear interpolation we used *Dierckx.jl*.

⁶ To construct a Delaunay tessellation we used *VoronoiDelaunay.jl*.

(Wagner & Pruß 2002), the density uncertainty is approximately 0.01 per cent (liquid and solid), 0.03 to 0.1 per cent (vapour), and up to 0.5 per cent in the region around and beyond the critical point. They give a more detailed breakdown of these errors in their section 6.3.2, in particular fig. 6.1. We estimate that the error beyond these regions is closer to 1 per cent if we extrapolate beyond the table and assume that the uncertainty continues to increase at higher temperatures and pressures. For the supercritical fluid, plasma and superionic phases in the data of French et al. (2009), they state that “the QMD EOS is accurate up to 1 per cent for the conditions relevant for the giant planet’s interiors of our solar system.” For the ice VII phase, the measurements of Sugimura et al. (2010) have errors of between 0.003 per cent and 0.5 per cent. Finally, it is not possible to give a meaningful uncertainty estimate at higher pressures where no measurements exist, but we do not treat the temperature dependence there anyway.

2.2.4 Thermal expansion and heat capacity

Equation 6 requires both a heat capacity c_p and a thermal expansion coefficient α (defined in equation 5). Following our goal of handling temperature effects appropriately, we explicitly sought out temperature-dependent forms for these.

We used the IAPWS tables for heat capacity in the liquid–vapour range, then took the nearest available data point from these tables for all other pressure–temperature points. This is because we could not find readily available heat capacity data across the full range of phases in our equation of state. This approach therefore does not reflect any changes in heat capacity between the high-pressure ice phases. The most significant effect is the change in heat capacity across the liquid–vapour phase boundary, which we do capture in our models.

We drew the thermal expansion coefficient α directly from the equation of state by evaluating equation 5. We used automatic differentiation⁷ where possible to evaluate the derivative. In some cases this was not possible⁸ so we used finite differencing⁹. As well as pre-computing the equation of state itself, we pre-computed and tabulated the thermal expansion coefficient on the same pressure–temperature grid. Some previous works have assumed a fixed thermal expansion coefficient: for example, Ehrenreich et al. (2006) took a fixed value for α in their models. We believe that our approach is more appropriate for understanding how the temperature gradient and physical properties of a watery planet are affected by the thermal properties of water.

⁷ We used forward-mode automatic differentiation provided by [ForwardDiff.jl](#).

⁸ The Delaunay triangulation method in the library we used incorporates a method called floating-point filtering, which relies on the specific properties of floating point numbers. It could not be used with the automatic differentiation approach we used, which evaluates functions as usual but replaces the inputs with a special numeric type.

⁹ We used the package [Calculus.jl](#).

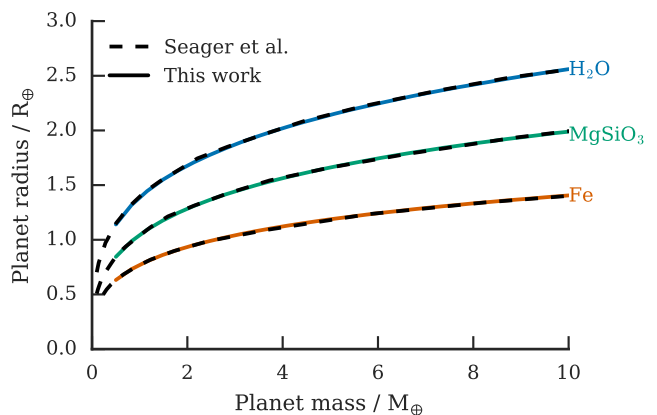


Figure 4. Validation of isothermal models. Our structural models exactly reproduce previous results in the isothermal case. Here we show mass–radius relations for homogeneous isothermal spheres. If we adopt identical equations of state to those used by Seager et al. (2007), we obtain the same result. This serves as a verification that we are correctly solving the structural equations. These models used zero surface pressure and have no temperature dependence: the equations of state are isothermal and are taken at 300 K.

2.3 Model verification

We verified our models by making mass–radius diagrams as described in the previous section and comparing them with previous work.

2.3.1 The isothermal case

We checked that our models work in the isothermal case by replicating the mass–radius relations of Seager et al. (2007). We exactly reproduced the mass–radius relations when we constructed homogeneous isothermal 300 K planets using the equations of state specified in their paper, as shown in Fig. 4. We set the surface pressure of our models to zero, following the boundary condition they used. The surface pressure hardly affects the results because the equations of state are for the solid phase only. This identical mass–radius relation verified that our integrator works correctly, and we therefore began to investigate where the differences lie upon including temperature effects.

2.3.2 The adiabatic case

We verified our adiabatic multi-layer models by comparing them with those of Valencia et al. (2007), who constructed similar models using the ice VII equation of state for water (Fig. 5). When we set high surface pressures (10^{10} Pa) we forced the surface layer of water to begin as ice VII or close to it and therefore produced a very similar mass–radius relation. However, we predict inflated radii at lower surface pressures and therefore conclude that surface temperature and surface pressure are both important factors for determining the radius of a planet with a water layer. We further explore this relationship in our results section.

There are minor differences between our mass–radius relations and the mass–radius relations presented by Valencia

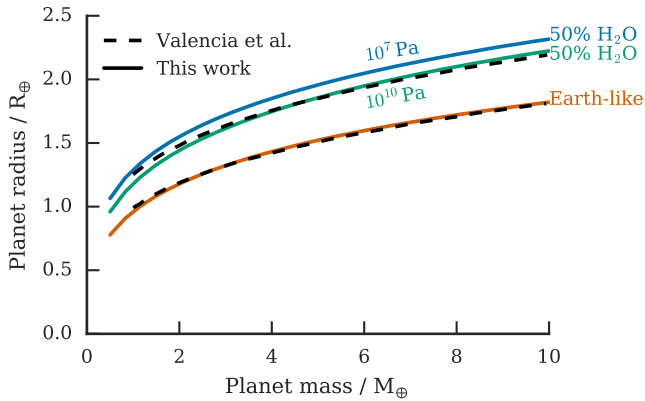


Figure 5. Validation of adiabatic models. Our mass–radius relations reproduce those for dry planets well, and predict inflated radii for planets with water layers. Here we show mass–radius relations for two classes of models: dry planets (33 per cent Fe and 67 per cent MgSiO_3 by mass), and wet planets (17 per cent Fe, 33 per cent MgSiO_3 , and 50 per cent water). We compared the mass–radius relations with the work of [Valencia et al. \(2007\)](#) who constructed models with ice VII layers. At a surface pressure of 10^{10} Pa the water layer in the wet planets is mostly ice VII and so our results are similar in this case. Small differences are likely due to our different equation of state choice for ice VII. However, at lower surface pressures, water can have an extended lower density shell that results in a larger planet than otherwise expected. The surface temperature in these models is 550 K, matching the characteristic temperature used by [Valencia et al. \(2007\)](#) in their models.

[et al. \(2007\)](#). We slightly underpredict the radii of lower-mass planets in models with surface pressures of 10^{10} Pa. These differences are likely due to our choice of equation of state: we use only simple isothermal prescriptions for iron and magnesium silicate and include more phases of water than just ice VII. We also did not include any treatment of conductive boundary layers in our models. In general, however, our results agree well with theirs.

We also compared our results with the evolutionary models of [Lopez et al. \(2012\)](#). Although we were able to reproduce their mass–radius relation for Earth-like planets, we were less successful when adding extended water layers (Fig. 6). We can match the radius of an arbitrary planet by choosing an appropriate surface pressure but we underpredict the radii of small planets and overpredict the radii of large planets compared with their results. This may be a result of different equation of state choices or different temperature gradients during the course of their evolutionary calculations.

Fig. 6 also provides a first indication of how changes in surface temperature can affect the mass–radius relation. We highlight the magnitude of these differences and note that they are still significant at pressures of 10^7 Pa (100 bar) and up, well into the pressure region where many atmospheric models terminate. We explore the effects on our models of changing surface temperature, surface pressure and composition in the next section.

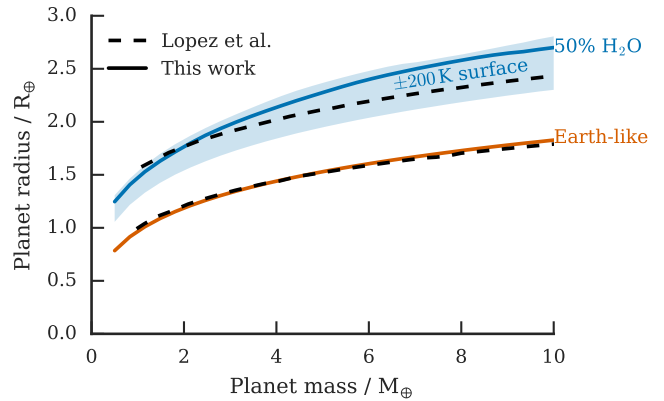


Figure 6. Comparison with evolutionary models. We plot dry (Earth-like) and wet (50 per cent water on an Earth-ratio core/mantle) mass–radius relations. Shown for comparison are models by [Lopez et al. \(2012\)](#), who build on work by [Fortney et al. \(2007\)](#) and [Nettelmann et al. \(2011\)](#) by using a thermal evolution approach to track the entropy within each planet as it cools. Surface temperature significantly alters the mass–radius relation in our models. The surface temperature in these models is 700 K but the shaded band shows models with surface temperatures from 500 to 900 K, a significant spread, which is caused by temperature-dependent density changes of water at lower pressures. We chose a surface pressure of 10^7 Pa to approximately match the radii of [Lopez et al. \(2012\)](#). Their method does not begin from an explicit surface pressure, as ours does.

3 RESULTS

We have explored the effects of temperature dependence on the radii of water-rich super-Earths. This section shows that significant radius variations can occur across temperature ranges relevant to super-Earths. We explored the dependence of super-Earth radii on three key model parameters.

1. Planet surface temperature, with the water layer temperature profile taken as

- a) isothermal, or
- b) adiabatic.

2. Planet surface pressure.

3. Planet composition, i.e. water mass fraction.

3.1 Effect of surface temperature on isothermal and adiabatic interiors

We found that thermal expansion can lead to significant changes in the radii of water-rich super-Earths. We constructed super-Earths in two different ways. First we modelled them as isothermal spheres containing an Earth-like core (33 per cent Fe and 67 per cent MgSiO_3) underneath a water layer of 30 per cent of the planet’s mass. Then we instead allowed the temperature to increase adiabatically into the water layer. Fig. 7 shows that the assumption that thermal expansion effects are negligible, which was made in some previous studies, is not the case. This is true in two senses. First, a significant temperature dependence exists when we adopt an adiabatic interior temperature profile compared with an isothermal one. The surface temperature also affects the radius of a planet within both types of models.

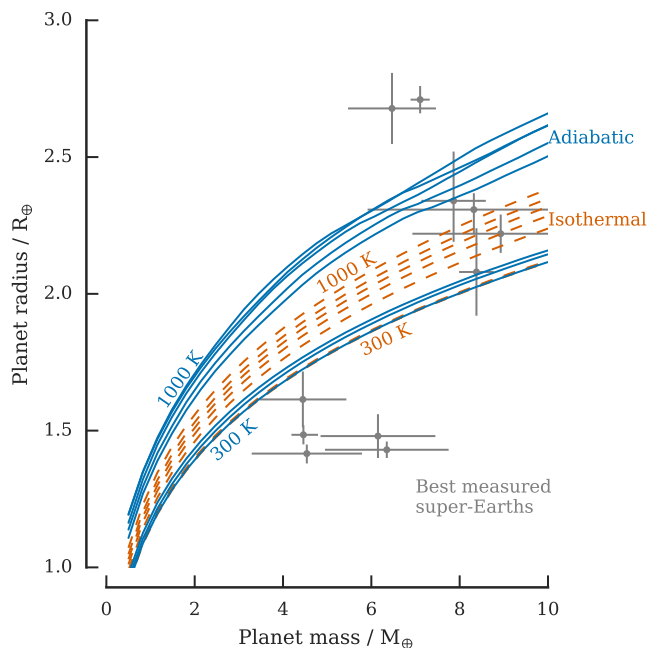


Figure 7. Dependence of watery super-Earth radii on surface temperature and internal temperature profile. An increased surface temperature results in an increased planetary radius. This effect is especially pronounced in the full adiabatic temperature treatment. Here we show super-Earths with an Earth-like core under a 30 per cent water layer by mass. We treated the temperature in two different ways: an isothermal treatment with a fixed constant temperature and an adiabatic treatment where we fixed the surface temperature but allowed the temperature to increase inwards according to the adiabatic relation (equation 6). The adiabatic models are warmer and therefore significantly larger overall, but even the isothermal planets display some radius change due to temperature. The effects of this temperature dependence are comparable to current uncertainties on measured masses and radii for some of the best-characterised exoplanets¹¹. The surface pressure in these models is 10^7 Pa (100 bar), and the temperature increases in steps of 100 K. The large gap between 500 and 600 K in the adiabatic case is due to a density discontinuity between the liquid and vapour phases.

The adiabatic models have a larger radius for a given mass when compared with the isothermal case. This is to be expected: the average temperature is higher along an adiabat than an isotherm fixed at the surface temperature, and the density of water generally decreases with temperature. The increase in radius is significant at higher surface temperatures, as shown in Fig. 7. For example, a $4M_{\oplus}$ 30 per cent water planet with a 600 K surface has a radius of $1.8R_{\oplus}$ if its water layer is isothermal, but $2R_{\oplus}$ if it is adiabatic. Across the super-Earth mass range we considered, the adiabatic radii increased by up to $0.3R_{\oplus}$ when compared with the isothermal case. The difference becomes particularly pronounced at higher surface temperatures, at which point the

water layer may consist of supercritical fluid rather than liquid, solid, or vapour (Fig. 1).

A significant dependence on surface temperature also exists when using the adiabatic models. That is, changing the surface temperature affects the radius of a model water super-Earth even when its temperature profile is already being treated as adiabatic. In the case of a $10M_{\oplus}$ planet, increasing the surface temperature from 300 to 1000 K gave a radius increase of $0.6R_{\oplus}$. For an Earth-mass planet the increase was approximately $0.3R_{\oplus}$ for the same temperature range.

We have highlighted above the change in the adiabatic models, which we claim are a more realistic representation of the actual temperature structure within the planet. But even the isothermal models show a significant increase in radius with the planet’s temperature. For a $10M_{\oplus}$ planet, the change in radius is $0.3R_{\oplus}$ from 300 to 1000 K. This is due to the thermal expansion of the planet as a whole, rather than of one small part of the water layer near the surface. We do not necessarily expect an adiabatic temperature gradient throughout the whole planet because the entire interior may not all be convective. For example, Valencia et al. (2007) included conductive boundary layers in their models. In that case, the true temperature-dependent behaviour of the mass–radius diagram might lie between the adiabatic and isothermal cases. Despite this, Fig. 7 shows that the surface temperature can still play an important role in determining the radius of a planet if it has a substantial water layer. This is true even in the extreme isothermal case where there is no temperature gradient at all within the planet.

These models have a surface pressure of 10^7 Pa (100 bar) so this effect is not due to the strong liquid–vapour transition at 1 bar. In fact, we still see these effects past the critical pressure of water (2.206×10^7 Pa). The critical point, which is visible in Figs 1 and 2, is the point in temperature–pressure space beyond which there is no distinct phase transition from liquid to vapour. This indicates that a liquid–vapour transition is not required to produce a significantly inflated radius when the water layer is heated. We discuss the effect of pressure on these models further in the next section.

3.2 Effect of surface pressure

The surface pressure can strongly affect the temperature-dependent thickness of the water layer (Fig. 8). For example, at high temperatures (1000 K), increasing the surface pressure of a 10 per cent water and $4M_{\oplus}$ planet from 10 bar to 1000 bar compresses the water layer significantly, decreasing the planet’s radius by a factor of two. And at low pressures we see a bifurcation in the surface pressure contours where a surface temperature increase of 100 K or less can inflate the radius of a watery super-Earth by more than 50 per cent. This is the result of a transition across the liquid–vapour phase boundary, which exists at pressures up to the critical pressure of water (2.206×10^7 Pa). Our interior structure code is most likely not the best choice for modelling such a quasi-atmospheric layer: we did not handle radiative energy transfer in our models. We have therefore not undertaken a detailed study of the behaviour of these vapour layers. They likely require a more sophisticated treatment of the temperature profile than our adiabatic assumption.

Despite observing highly inflated radii when the tem-

¹¹ These data are from exoplanets.org. We selected planets with known radii and masses of 1 to $10M_{\oplus}$. We then plotted the twelve planets with the lowest summed relative uncertainty in mass and radius ($\Delta R/R + \Delta M/M$).

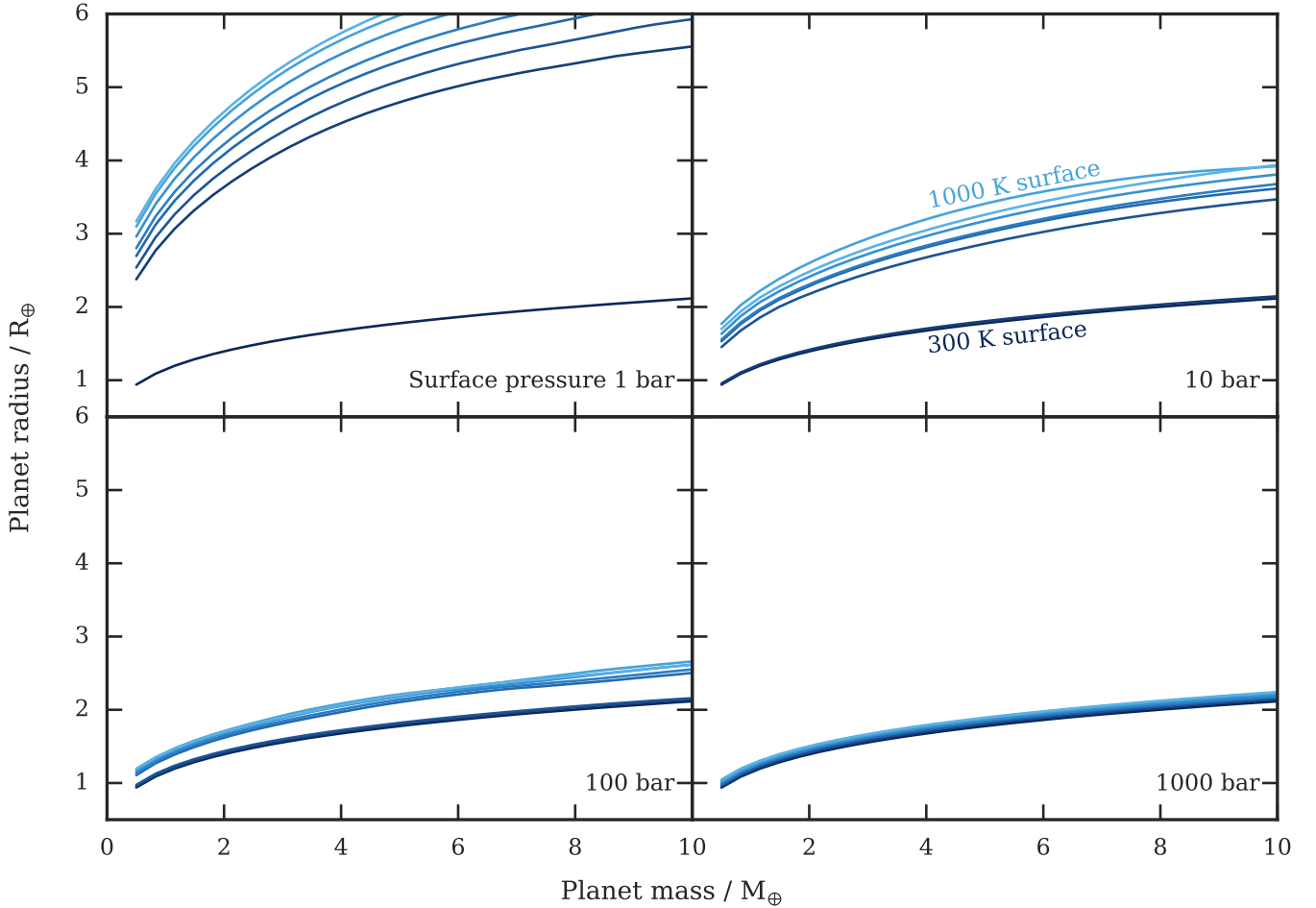


Figure 8. Dependence of radii on surface pressure. The effect of temperature on the radius of watery planets decreases with increasing surface pressure, but remains significant (greater than about $0.1R_{\oplus}$) for pressures below 1000 bar. Here we show mass–radius relations for spheres with an Earth-like core under a 30 per cent water layer, changing only the surface pressure each time. The temperature dependence remains even beyond the critical pressure of water (2.206×10^7 Pa), at which point the surface water exists as a supercritical fluid. Only at very high pressures (10^9 or 10^{10} Pa; 10000 or 100000 bar) does this temperature dependence vanish.

perature is increased across the liquid–vapour phase boundary, we still see temperature-dependent variation in the planet’s radius past the critical pressure of water. This is because the density of water is still strongly temperature-dependent in the super-critical regime. In fact, we might reasonably expect the same inflated radii in any situation where the pressure of the water layer places it in a region of the water phase diagram that has significant temperature dependence. If the water layer is heated to thousands of Kelvin, this temperature dependence may only begin to disappear around 10^{10} Pa (100000 bar, Fig. 3). At a pressure of 10^8 Pa (1000 bar), a watery super-Earth with a surface temperature of 1000 K still has a radius that is up to $0.1R_{\oplus}$ larger than one with a surface temperature of 300 K. This is comparable to or greater than the best current uncertainties on measured super-Earth radii (Fig. 7), and indicates that the surface temperature is a key parameter to consider when one attempts to model planets with significant water mass.

We included no atmospheric layers in these models. Other studies have provided more complete treatments of atmospheric layers. For example, [Rogers & Seager \(2010b\)](#)

included a gas layer on top of an isothermal interior structure model in order to interpret the structure of the planet GJ 1214b. And [Valencia et al. \(2013\)](#) used internal structure models coupled with an atmospheric layer, exploring the dependence of radii on various model parameters including equilibrium temperature and water content. Given that we set the surface pressure to between 10^5 and 10^{10} Pa (1 and 100000 bar), our models must therefore represent the layers interior to an atmosphere of some sort.

3.3 Effect of water content

We find that changing the water content does not significantly affect the temperature-dependent behaviour discussed in earlier sections (Fig. 9). We constructed planets with water, silicate, and iron layers, fixing the silicate:iron mass ratio to the Earth value of 2:1 and allowing the water shell to vary in mass. These models correspond to an Earth-like nucleus with an extended water layer at the surface.

The effects of surface temperature on radius are comparable in magnitude across all our models with water layers,

even when we set the water layer mass to just 1 per cent of the mass of the entire planet. For a $10M_{\oplus}$ super-Earth with a surface pressure of 10^7 Pa (100 bar), the radial change when the surface temperature increases 300 to 1000 K is $0.5R_{\oplus}$ (for a 50 per cent water planet) and $0.4R_{\oplus}$ (for a 1 per cent water planet). This similarity holds across the entire range of planetary masses we considered. This suggests that the bulk of the radius change comes from a water layer on the surface whose density depends strongly on the surface temperature.

3.4 Effect of temperature dependence on phase structure

Our adiabatic assumption provides for water layers which span different phases depending on the pressure–temperature profile. As previously noted, we observed a significant bifurcation in the mass–radius diagrams when the surface temperature crossed the condensation curve of water. As an example of how the surface temperature affects the structure of a planet at pressures beyond the critical pressure of water, Fig. 10 shows pressure–temperature profiles for adiabatic spheres of water with different surface temperatures. The planet contains a significant ice VII component when the surface temperature is low. But at high surface temperatures the centre of the planet may consist mostly of the superionic or plasma phases of water, which are shown in Figs 1 and 2.

Others have explored the layered phase structure of watery planets (e.g. Zeng & Sasselov 2014; Ehrenreich et al. 2006). In particular, Ehrenreich et al. (2006) included an analysis of radiogenic heating in their models to assess the feasibility of having a liquid ocean under a cold ice shell.

Though we have not assessed how the layered phase structure of a planet’s water layer might affect other properties of the planet, the phase of water could be important for its potential to sustain convective energy transport or magnetic fields (Zeng & Sasselov 2014). We did include a more complete treatment of the thermal expansion coefficient α (calculating it directly from the equation of state) and the variable heat capacity c_p . This approach may result in a phase structure that differs from other studies. In future we anticipate investigating this more closely to assess whether these internal energy sources are indeed sufficient to drive convection throughout our models: is the assumption of a fully convective interior reasonable? As a first indication of this, we consider the fact that we do not find major deviations from the mass–radius relations of Valencia et al. (2007) (Fig. 5) to be promising. This is despite the fact that they include conductive boundary layers in their models.

The phase structure is also of interest when we consider questions of habitability. The properties of water change significantly near the critical point: water becomes a low-dielectric fluid and a poor solvent for polar substances (Ansimov et al. 2004). The nature of reactions supported by water is also expected to change at high temperatures (Kruse & Dinjus 2007). We would expect significant changes in any kind of life that could be found within these water layers, both when compared with liquid oceans on Earth and when seen over time as the planet’s structure evolved.

4 CONCLUSION AND DISCUSSION

In this paper we have presented planetary interior structure models of water-rich super-Earths. The models incorporate a temperature-dependent water equation of state and use an adiabatic treatment for the temperature gradient. In doing so, we synthesized an updated equation of state for water which attempts to capture all the relevant temperature-dependent behaviour. We directly calculated the thermal expansion coefficient α from the equation of state, rather than treating it as a constant, and we used a variable heat capacity based on experimental data. Our conclusions are as follows.

First, when one models a solid planet, adding a water layer comes with a substantial thermal dependence. By this we mean that the temperature of the planet may substantially alter the radius of the planet as the water layer expands and contracts. Previous studies have shown that including a temperature gradient in Earth-like planets produces a minimal change in its radius (Howe et al. 2014; Grasset et al. 2009; Seager et al. 2007). We showed that this assumption no longer holds once large water layers are considered, even setting aside the unrealistic case of a 100 per cent water planet. For example, consider the case of a $4M_{\oplus}$ planet with an Earth-like core underneath a water layer of 5 per cent of the planet’s total mass. If the surface pressure is 10^7 Pa (100 bar), the difference in the planet’s radius when the surface is heated from 300 K to 1000 K is approximately $0.3R_{\oplus}$ (Fig. 9). This effect is on top of any thermal expansion of iron and silicate: our models treated the rocky layers as isothermal. It is also in addition to any uncertainty in the equation of state itself. Such changes in radii are significant considering that current observations can already measure super-Earth radii to precisions better than $0.1R_{\oplus}$ (e.g. Fig. 7).

The strength of the planet radius–temperature relation also depends on the surface pressure. This is a result of the decreasing thermal expansion of water with pressure: the coefficient of thermal expansion is much smaller in high-pressure ice than in the liquid, vapour, or supercritical fluid phases. At pressures of more than about 10^{10} Pa (100 000 bar) the radial temperature dependence becomes irrelevant: the uncertainty in current planetary radius measurements is larger than any conceivable radial change owing to temperature effects, so more precise structural models may not be useful. However, there is still a significant radial dependence on temperature at lower surface pressures. At 10^8 Pa (1000 bar), a watery super-Earth with a surface temperature of 1000 K can be up to $0.1R_{\oplus}$ larger than one with a surface temperature of 300 K. It is therefore important to include temperature effects in the interior models if an accurate radius is required as part of the model.

This pressure dependence manifests itself most strongly below the critical point of water. At pressures below this critical pressure, a phase transition still exists between liquid and vapour. There is therefore a bifurcation in the mass–radius diagram: a small increase in surface temperature can cause a large change in radius (up to a factor of two) as the surface water vaporises. We caution that it is likely not appropriate to attempt to treat such vapour layers using our approach, which is intended for interior structures. However,

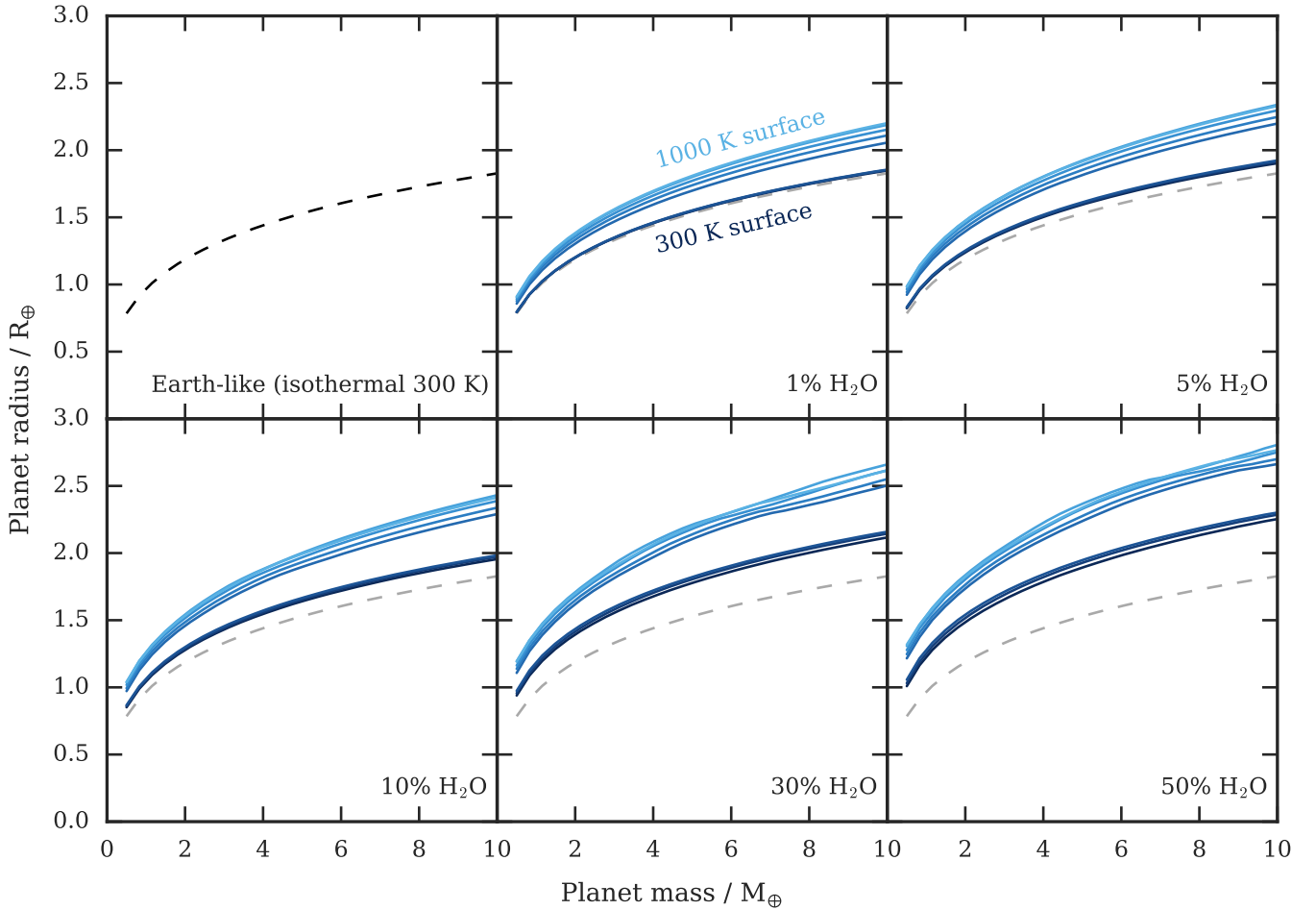


Figure 9. Dependence of radii on water mass fraction. Even low-mass water layers result in planets that are strongly affected by temperature changes, especially when water on the surface is hot enough to be in the vapour or supercritical phase. Here we show mass–radius relations for multi-layer planets: an iron core with silicate and (in all but the first panel) water layers. We show the Earth-like iron-silicate core in each panel for comparison. All the watery planets are larger than the dry case owing to the lower density of water. Surface temperature variation affects the radius of a watery planet by a similar amount in each case, and it can increase the radius by up to 25 per cent. Because the iron and silicate layers are isothermal, this variation is due solely to temperature effects in the water layer. We fixed the silicate:iron mass ratio at 2:1 and set the surface pressure to 10^7 Pa (100 bar). The temperature contours are in steps of 100 K.

a lesser version of this effect is still visible at higher pressures.

We consider the surface pressure as a free parameter in our models. In principle, the surface pressure could be constrained through spectroscopic observations of the planetary atmosphere, though such observations are currently difficult for super-Earths. The surface pressure is set by the depth beyond which atmospheric measurements can no longer probe. [Madhusudhan & Redfield \(2015\)](#) discussed planets with water-rich atmospheres, describing the use of measurements both in and out of opacity windows to determine the atmospheric thickness. The pressure to which these measurements probe varies from 0.1 bar (in regions of high opacity; that is, outside an atmospheric window) to 100 bar (within such a window). Our models go beyond this pressure range, and are therefore appropriate to treat the structure of the planet below the observable opacity surface.

In the case of a volatile layer such as water, the line between interior and atmosphere can become blurred. The

picture is complicated by atmospheric effects that can increase the opacity. If a cloud layer forms in the atmosphere, the opacity surface may not necessarily be at the same depth or pressure as any solid surface of the planet. Turbidity effects around the critical point may also affect the opacity. It is for this reason that high-temperature exoplanets are interesting: at higher temperatures, a cloud deck is less likely to occur and atmospheric measurements are therefore able to probe deeper. The previously-mentioned opacity windows may therefore be able to provide a view through the atmosphere to the planet’s surface, or at least to a point where the assumption of interior convective mixing is more likely to hold.

We therefore conclude that, in some cases, planetary heating may alter the interpretation of a planet’s radius if a water layer is part of the model. This is especially true if the planet consists entirely of water, but this is an unlikely physical scenario. More importantly, the result is still significant even if the surface of the water layer is at moderately

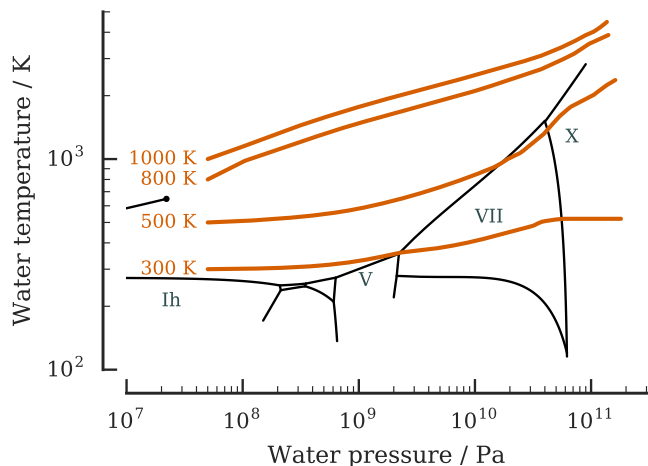


Figure 10. Model pressure–temperature profiles. Increasing the surface temperature means that more of the planet consists of superionic or plasma phases of water, with the transition to high-pressure ice happening deeper within the interior or not at all. Here we show pressure–temperature profiles for $3M_{\oplus}$ spheres of water with a surface pressure of 5×10^7 Pa, which is beyond the critical pressure. At a surface temperature of 300 K, the planet consists of liquid water over an ice VII core. But the ice VII phase may not be present within the interior at higher surface temperatures. Instead, the bulk of the planet consists of water in the superionic or plasma state. This, combined with the low-density supercritical fluid at the surface, results in an inflated radius.

high pressures and lies underneath a heavy atmosphere. All that is required for the water layer’s density to change significantly from the isothermal case is for a temperature increase of a few hundred Kelvin. Moreover, even isothermal watery planets have some degree of radial temperature dependence: up to $0.3R_{\oplus}$ across the mass range of super-Earths and in the temperature range of 300 to 1000 K.

Understanding how the mass–radius relation can be affected by temperature allows us to take the step of detecting and characterising water-rich planets, taking their surface temperatures into account while modelling them. This is an important precursor to narrow the search to planets that would be considered more classically habitable. It will be especially useful in the context of the next generation of super-Earths expected to be found orbiting bright stars by missions such as PLATO (Rauer et al. 2014), TESS (Ricker et al. 2014) and CHEOPS (Broeg et al. 2013). This approach is promising because it is linked to the characteristic equilibrium temperature, which can be determined from observations of the planet, and so can be included in analyses of populations of planets. Through this we might better understand what proportion of planets include substantial water content.

The temperature dependence is also important to take into account in approaches such as that of Kipping et al. (2013), where a watery interior model is used to place a lower bound on the atmospheric height of an observed planet. We have shown that the radius of an adiabatic watery planet may be significantly higher than the zero-temperature or isothermal case. Incorporating a surface temperature esti-

mate into this approach should therefore give better constraints.

From an observational perspective, these results are most interesting at intermediate pressures. At low pressures (10^5 Pa or 1 bar) we cannot claim that we accurately capture the behaviour of what is now essentially an atmosphere, because we include no prescription for radiative energy transport in our models. At high pressures (10^{10} Pa or 100 000 bar) any temperature dependence in the water equation of state disappears. The physical scenario most relevant for these models is therefore that of a water layer (ocean, ice or supercritical fluid) underneath a thin or moderate atmosphere. Others such as Rogers & Seager (2010b) have already included volatile layers on top of interior structure models. Adding more complete temperature dependence to the interior portion of these planetary models is a worthwhile future direction if we wish to treat them as water-rich.

We look forward to two developments in particular. The first is improved atmospheric characterisation and modelling, which will provide useful pressure and temperature boundary conditions at the base of the atmosphere. The question of interior–atmospheric interactions is a rich one that is only starting to be explored. Integrating atmospheric and interior models promises progress on questions about surface chemistry, outgassing and other processes that can shape the atmosphere of a planet. The second development that will make use of this work is improved spectral resolution of atmospheric observations, and in particular the ability to seek out atmospheric windows (Madhusudhan & Redfield 2015). By observing at wavelengths which pass through the atmosphere, we can in principle directly measure the radius of any solid interior underneath that atmosphere and thus have a better starting point for interpreting the interior structure.

ACKNOWLEDGEMENTS

We thank the anonymous reviewer for an insightful review and Christopher Tout for helpful discussions and comments. ST gratefully acknowledges support from the Royal Society of New Zealand.

REFERENCES

- Ansimov M. A., Sengers J. V., Sengers J. M. L., 2004, in Fernandez-Prini R., Harvey A., Palmer D., eds, , *Aqueous Syst Elev Temp Press*. Elsevier Academic Press, London, Chapt. 2, p. 29
- Baraffe I., Chabrier G., Barman T. S., 2008, *A&A*, 482, 315
- Baraffe I., Chabrier G., Fortney J. J., Sotin C., 2014, in Beuther H., Klessen R. S., Dullemond C. P., Henning T., eds, , *Protostars Planets VI*. University of Arizona Press, Tucson, pp 763–786, doi:10.2458/azu_uapress_9780816531240
- Belonoshko A., Saxena S., 1991, *Geochim Cosmochim Acta*, 55, 381
- Broeg C., et al., 2013, *EPJ Web Conf*, 47, 03005
- Choukroun M., Grasset O., 2007, *J Chem Phys*, 127, 124506
- Dorn C., Khan A., Heng K., Connolly J. A. D., Alibert Y., Benz W., Tackley P., 2015, *A&A*, 577, A83

- Dunaeva A. N., Antsyshkin D. V., Kuskov O. L., 2010, *Sol Syst Res*, 44, 202
- Ehrenreich D., Lecavelier des Etangs A., Beaulieu J., Grasset O., 2006, *ApJ*, 651, 535
- Fei Y., Mao H.-k., Hemley R. J., 1993, *J Chem Phys*, 99, 5369
- Feistel R., Wagner W., 2006, *J Phys Chem Ref Data*, 35, 1021
- Fortney J. J., Nettelmann N., 2009, *Space Sci Rev*, 152, 423
- Fortney J. J., Marley M. S., Barnes J. W., 2007, *ApJ*, 659, 1661
- Frank M. R., Fei Y., Hu J., 2004, *Geochim Cosmochim Acta*, 68, 2781
- French M., Mattsson T., Nettelmann N., Redmer R., 2009, *PRB*, 79, 054107
- Grasset O., Schneider J., Sotin C., 2009, *ApJ*, 693, 722
- Guillot T., 1999, *Planet Space Sci*, 47, 1183
- Haghighipour N., 2011, *Contemp Phys*, 52, 403
- Howe A. R., Burrows A. S., Verne W., 2014, *ApJ*, 787, 26
- Hubbard W. B., MacFarlane J. J., 1980, *J Geophys Res*, 85, 225
- Hubbard W., Marley M. S., 1989, *Icarus*, 78, 102
- Kipping D. M., Spiegel D. S., Sasselov D. D., 2013, *MNRAS*, 434, 1883
- Knudson M. D., Desjarlais M. P., Lemke R. W., Mattsson T. R., French M., Nettelmann N., Redmer R., 2012, *PRL*, 108, 091102
- Kruse A., Dinjus E., 2007, *J Supercrit Fluids*, 39, 362
- Levi A., Sasselov D., Podolak M., 2014, *ApJ*, 792, 125
- Lopez E. D., Fortney J. J., Miller N., 2012, *ApJ*, 761, 59
- Lyon S. P., Johnson J. D., 1992, Technical report, SESAME: The Los Alamos National Laboratory equation of state database. LA-UR-92 3407, Los Alamos National Lab
- Madhusudhan N., 2012, *ApJ*, 758, 36
- Madhusudhan N., Redfield S., 2015, *Int J Astrobiol*, 14, 177
- Madhusudhan N., Lee K. K. M., Mousis O., 2012, *ApJ*, 759, L40
- Milone E. F., Wilson W. J., 2014, *Solar System Astrophysics: Background Science and the Inner Solar System*, 2 edn. Springer, New York, doi:10.1007/978-1-4614-8848-4
- Mordasini C., Alibert Y., Georgy C., Dittkrist K.-M., Klahr H., Henning T., 2012, *A&A*, 547, A112
- More R. M., Warren K. H., Young D. A., Zimmerman G. B., 1988, *Phys Fluids*, 31, 3059
- Nettelmann N., Holst B., Kietzmann A., French M., Redmer R., Blaschke D., 2008, *ApJ*, 683, 1217
- Nettelmann N., Fortney J. J., Kramm U., Redmer R., 2011, *ApJ*, 733, 2
- Owen J. E., Wu Y., 2015, preprint (arXiv:1506.02049)
- Poirier J.-P., 2000, *Introduction to the Physics of the Earth's Interior*, 2nd edn. Cambridge University Press, Cambridge
- Press W. H., 2007, *Numerical Recipes: The Art of Scientific Computing*, 3rd edn. Cambridge University Press, Cambridge
- Rauer H., et al., 2014, *Exp Astron*, 38, 249
- Redmer R., Mattsson T. R., Nettelmann N., French M., 2011, *Icarus*, 211, 798
- Ricker G. R., et al., 2014, in Oschmann J. M., Clampin M., Fazio G. G., MacEwen H. A., eds., Vol. 9143, *Proc SPIE*. pp 914315–914320 (arXiv:1406.0151), doi:10.1117/12.2063489, http://arxiv.org/abs/1406.0151
- Rogers L. A., 2015, *ApJ*, 801, 41
- Rogers L. A., Seager S., 2010a, *ApJ*, 712, 974
- Rogers L. A., Seager S., 2010b, *ApJ*, 716, 1208
- Rogers L. A., Seager S., 2012, Phd thesis, MIT
- Salpeter E., Zapolsky H., 1967, *PR*, 158, 876
- Seager S., Kuchner M., Hier-Majumder C. A., Militzer B., 2007, *ApJ*, 669, 1279
- Senft L. E., Stewart S. T., 2008, *Meteorit Planet Sci*, 43, 1993
- Sotin C., Grasset O., Mocquet A., 2007, *Icarus*, 191, 337
- Sotin C., Jackson J. M., Seager S., 2010, in Seager S., ed., *Exoplanets*. University of Arizona Press, Chapt. 16, pp 375–395
- Stewart S. T., Ahrens T. J., 2005, *J Geophys Res*, 110, E03005
- Sugimura E., Komabayashi T., Hirose K., Sata N., Ohishi Y., Dubrovinsky L. S., 2010, *PRB*, 82, 134103
- Thompson S. L., Lauson H. S., 1972, Technical report, Improvements in the Chart B radiation hydrodynamic code III: revised analytic equations of state. SC-RR-71 0714, Sandia National Lab
- Unterborn C. T., Dismukes E. E., Panero W. R., 2015, preprint (arXiv:1510.07582)
- Valencia D., O'Connell R. J., Sasselov D. D., 2006, *Icarus*, 181, 545
- Valencia D., Sasselov D. D., O'Connell R. J., 2007, *ApJ*, 665, 1413
- Valencia D., Ikoma M., Guillot T., Nettelmann N., 2010, *A&A*, 516, A20
- Valencia D., Guillot T., Parmentier V., Freedman R. S., 2013, *ApJ*, 775, 10
- Vazan A., Kovetz A., Podolak M., Helled R., 2013, *MNRAS*, 434, 3283
- Vinet P., Smith J., Ferrante J., Rose J., 1987, *PRB*, 35, 1945
- Wagner W., Pruff A., 2002, *J Phys Chem Ref Data*, 31, 387
- Wagner F., Sohl F., Hussmann H., Grott M., Rauer H., 2011, *Icarus*, 214, 366
- Wilson H. F., Militzer B., 2012, *ApJ*, 745, 54
- Wilson H., Wong M., Militzer B., 2013, *PRL*, 110, 151102
- Zapolsky H. S., Salpeter E. E., 1969, *ApJ*, 158, 809
- Zeng L., Sasselov D. D., 2013, *PASP*, 125, 227
- Zeng L., Sasselov D. D., 2014, *ApJ*, 784, 96

This paper has been typeset from a \LaTeX file prepared by the author.